

Efficient organic solar cells with the active layer fabricated from glovebox to ambient condition

Cite as: Appl. Phys. Lett. **117**, 133301 (2020); <https://doi.org/10.1063/5.0021509>

Submitted: 11 July 2020 . Accepted: 17 September 2020 . Published Online: 01 October 2020

Hengyue Li,  Keqing Huang, Yanan Dong, Xiaotong Guo, Yu Yang,  Qun Luo, Chang-Qi Ma, Dongfan Li, 
Guanghao Lu,  Jian Xiong, Jian Zhang,  Yingguo Yang, Xingyu Gao, and  Junliang Yang



View Online



Export Citation



CrossMark

ARTICLES YOU MAY BE INTERESTED IN

[Electronic-ionic coupling in perovskite based solar cells: Implications for device stability](#)
Applied Physics Letters **117**, 133904 (2020); <https://doi.org/10.1063/5.0023902>

[Emerging circularly polarized thermally activated delayed fluorescence materials and devices](#)
Applied Physics Letters **117**, 130502 (2020); <https://doi.org/10.1063/5.0021127>

[Spin valves as magnetically switchable spintronic THz emitters](#)
Applied Physics Letters **117**, 132407 (2020); <https://doi.org/10.1063/5.0025746>



Your Qubits. Measured.

Meet the next generation of quantum analyzers

- Readout for up to 64 qubits
- Operation at up to 8.5 GHz, mixer-calibration-free
- Signal optimization with minimal latency

Find out more



Efficient organic solar cells with the active layer fabricated from glovebox to ambient condition

Cite as: Appl. Phys. Lett. **117**, 133301 (2020); doi: [10.1063/5.0021509](https://doi.org/10.1063/5.0021509)

Submitted: 11 July 2020 · Accepted: 17 September 2020 ·

Published Online: 1 October 2020



View Online



Export Citation



CrossMark

Hengyue Li,¹ Keqing Huang,¹ Yanan Dong,¹ Xiaotong Guo,¹ Yu Yang,¹ Qun Luo,² Chang-Qi Ma,² Dongfan Li,³ Guanghao Lu,³ Jian Xiong,⁴ Jian Zhang,⁴ Yingguo Yang,⁵ Xingyu Gao,⁵ and Junliang Yang^{1,a)}

AFFILIATIONS

¹Hunan Key Laboratory for Super-Microstructure and Ultrafast Process, School of Physics and Electronics, Central South University, Changsha 410083, China

²Printable Electronics Research Center, Suzhou Institute of Nano-Tech and Nano-Bionics, Chinese Academy of Sciences, Suzhou 215123, China

³Frontier Institute of Science and Technology, Xi'an Jiaotong University, Xi'an 710054, China

⁴School of Material Science and Engineering, Guilin University of Electronic Technology, Guilin 541004, China

⁵Shanghai Institute of Applied Physics, Chinese Academy of Science, 2019 Jialuo Road, Shanghai 201800, China

^{a)} Author to whom correspondence should be addressed: junliang.yang@csu.edu.cn. Tel.: +86-731-88660256

ABSTRACT

Organic solar cells (OSCs) have been attracting considerable interest due to their unique advantages of low cost, light weight, and especially mechanical flexibility. The low-cost and high-throughput techniques matching with the large-scale and roll-to-roll (R2R) process for fabricating efficient OSCs in the ambient condition would greatly accelerate the potential commercialization of OSCs. Herein, we demonstrate that the fabrication processes of OSCs using the bulk heterojunction (BHJ) composed of poly[(2,6-(4,8-bis(5-(2-ethylhexyl)thiophen-2-yl)-benzo[1,2-b:4,5-b']dithiophene))-alt-(5,5-(1',3'-di-2-thienyl-5',7'-bis(2-ethylhexyl)benzo[1',2'-c:4'5'-c']dithiophene-4,8-dione))] (PBDB-T) and 3,9-bis(2-methylene-(3-(1,1-dicyanomethylene)-5-methylindanone)-5,5,11,11-tetrakis(4-hexylphenyl)-dithieno[2,3-d:2',3'-d']-s-indaceno[1,2-b:5,6-b']-dithiophene (IT-M)) are transferred from a glovebox to the ambient condition, where the deposition of doctor blading instead of conventional spin coating is investigated. The morphology, microphase separation, and crystallinity of BHJ PBDB-T:IT-M are dramatically influenced by the fabrication processes. The OSCs with a structure of ITO/ZnO/PBDB-T:IT-M/MoO₃/Ag fabricated via doctor-blading in the ambient condition show a power conversion efficiency (PCE) of 9.0% as compared to conventional spin-coated OSCs in a glovebox with a PCE of 11.91% and in the ambient condition with a PCE of 9.91%. These results suggest that efficient OSCs could be processed in the ambient condition by large-scale and low-cost doctor-blading, which can be compatible with the R2R manufacturing process.

Published under license by AIP Publishing. <https://doi.org/10.1063/5.0021509>

Organic solar cells (OSCs) are attracting much attention and have achieved significant progress as great potential candidates for promising future renewable energy sources due to the merits of light weight, low cost, solution-process ability, and large-scale roll-to-roll (R2R) manufacturing on a flexible substrate.^{1–10} With a rapid development in material synthesis, interface engineering, and design of the device structure, impressive progress on power conversion efficiencies (PCEs) has been reported.^{11–15} Very recently, the PCEs of state-of-the-art OSCs have surpassed 16% for single junction devices and 17% for tandem devices.^{16,17} However, most research on high-performance OSCs is fabricated in a smaller size in the glovebox via spin coating [as shown in Fig. 1(a)], which wastes a lot of material and is not compatible with large-scale mass production.^{18–20}

It is well known that there are some issues for fabricating OSCs with compatible large-scale deposition techniques from the lab-scale small area to a large area in the ambient condition, for example, the thickness-sensitive active layer,^{21,22} the large sheet resistivity of the normally used indium tin oxide (ITO) electrode,²³ halogenated solvents,^{24,25} module designs, and coating techniques.²⁵ Scalable printing techniques including doctor-blading, slot-die coating, and micro-gravure printing are developed rapidly, which exhibit the advantages of high throughput, high ratio of material utilization, manufacturing energy-efficiency, low cost, and matching with flexible substrates.^{26,27} Doctor-blading, as shown in Fig. 1(a), is a robust and reproducible deposition technique that can be employed in a large-scale, R2R process of OSCs with a high-quality film and good device

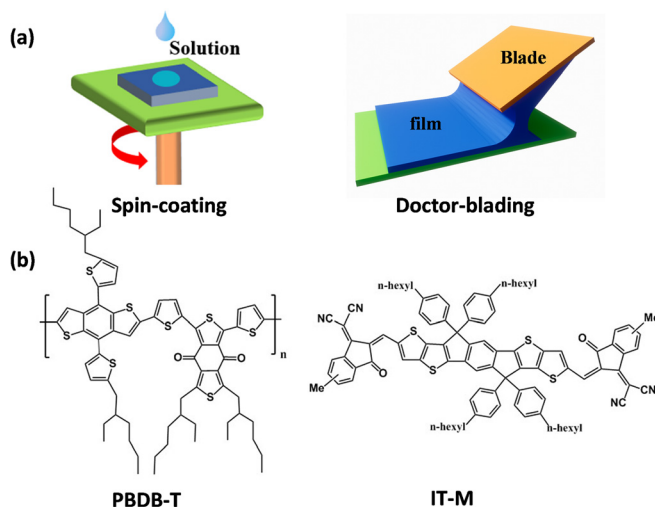


FIG. 1. (a) Schematics of spin-coating and doctor-blading deposition. (b) Chemical structures of PBDB-T and IT-M molecules.

performance.^{28–30} Recently, OSCs using the PBDB-T:TSR:[6,6]-phenylC71-butyric acid methyl ester (PC₇₁BM) bulk heterojunction as the active layer processed by doctor-blading exhibit a high PCE of 8.4% in the ambient condition,³¹ and OSCs using the poly[4,8-bis[5-(2-ethylhexyl)-2-thienyl] benzo[1,2-b:4,5-b']dithiophene-alt-(4-(2-ethylhexyl)-3-fluorothiopheno[3,4-b] thiophene)-2-carboxylate-2-6-diyl] (PTB7-Th):PC₇₁BM bulk heterojunction as the active layer fabricated by doctor-blading achieve a PCE of 8.31% in the ambient condition.³² On the other hand, non-fullerene OSCs show a breakthrough and rapid evolution because of non-fullerene acceptors with great absorption, tunable molecular energy levels, and superior optoelectronic properties.³³ It is reported that doctor-bladed OSCs based on PTB7-Th and non-fullerene acceptor 3,9-bis(2-methylene-(3-(1,1-dicyanomethylene)-indanone))-5,5,11,11-tetrakis(4-hexylphenyl)-dithieno[2,3-d:2',3'-d']-s-indaceno[1,2-b:5,6-b']dithiophene (ITIC) exhibit the PCEs up to 9.54% and 7.6% for the 0.14 cm² active area on ITO/glass and 2.03 cm² active area on the flexible ITO-free substrate in the glovebox, respectively.³⁴ Furthermore, a PCE up to 10.03% is achieved for doctor-bladed OSCs in the ambient condition using the poly[(2,6-(4,8-bis(5-(2-ethylhexyl)thiophen-2-yl)-benzo[1,2-b:4,5-b']dithioph-ene))-alt-(5,5-(1',3'-di-2-thien-yl-5',7'-bis(2-ethylhexyl)-benzo[1',2'-c:4'5'-c']dithioph-ene-4,8-dione))] (PBDB-T):ITIC bulk heterojunction as the active layer.³⁵ Meanwhile, efficient OSCs with a PCE of 10.0% via temperature-controlled slot-die coating and with a PCE of 7.11% on the flexible substrate via hot-deposition R2R processes were achieved.³⁶ The combined R2R process and slot-die coating were used to fabricate OSCs with sputtered silver electrodes on flexible PET, resulting in ITO-free OSCs with a PCE of 5.5%.³⁷

In this work, non-fullerene OSCs based on wide bandgap conjugated polymer PBDB-T and a non-fullerene small molecule acceptor 3,9-bis(2-methylene-(3-(1,1-dicyanomethylene)-5-methylindanone))-5,5,11,11-tetrakis(4-hexylphenyl)-dithieno[2,3-d:2',3'-d']-s-indaceno[1,2-b:5,6-b']-dithiophene (IT-M) [Fig. 1(b)] are fabricated by spin-coating in the glovebox, spin-coating in the ambient condition, and doctor-blading in the ambient condition, respectively. It is noted

that the active layers are annealed in the glovebox. MoO₃ and Ag electrodes are sequentially evaporated on the active layers. Then, the deposition technique (spin-coating or doctor blading) and conditions (in the glovebox or in the ambient condition) obviously influence the morphology and crystallinity of BHJ PBDB-T:IT-M thin films, and OSCs with a structure of ITO/ZnO/PBDB-T:IT-M/MoO₃/Ag [Fig. 2(a)] fabricated via doctor-blading in the ambient condition show a PCE of 9.00% as compared to spin-coated OSCs in the glovebox with a PCE of 11.91% and in the ambient condition with a PCE of 9.91%. The OSCs with high performance are promising to be produced in the industrial field. The transfer fabrication of OSCs with high performance from spin-coating in the glovebox to scaling up in the ambient condition is a very important step. These results exhibit excellent prospects to realize high-performance, large-area OSC devices fabricated via the large-scale doctor-blading technique matching with the R2R manufacturing process in the ambient condition.

The absorption spectra of PBDB-T and IT-M thin films are presented in Fig. S1. The PBDB-T exhibits strong absorption between 550 and 650 nm, while IT-M shows strong absorption at 600 and 750 nm. Thus, they show excellent complementary light absorption. The absorption spectra of PBDB-T:IT-M bulk heterojunction thin films deposited via spin-coating and doctor blading are shown in Fig. 2(b). The results suggest that spin-coated and doctor-bladed PBDB-T:IT-M bulk heterojunction thin films show similar absorption spectra. The doctor-bladed thin film in the ambient condition shows stronger absorption from 300 nm to 500 nm as compared with the spin-coated thin film fabricated in the ambient condition. In Fig. S1, the donor PBDB-T exhibits better absorption than acceptor IT-M in the wavelength range of 300–500 nm. Thus, it probably contributes that the donor PBDB-T is rich in the blend film fabricated by doctor blading.

The typical photovoltaic properties of spin-coated and doctor-bladed OSCs in the glovebox and ambient condition with a configuration of ITO/ZnO/PBDB-T:IT-M/MoO₃/Ag are shown in Fig. 2(c),

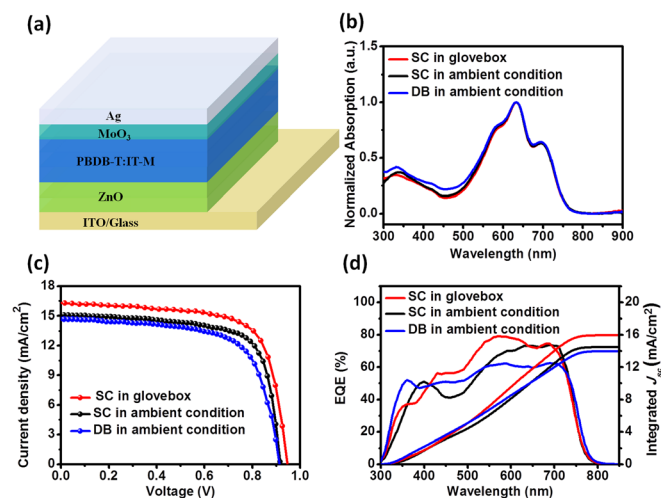


FIG. 2. (a) Schematic of the OSC architecture. (b) Normalized UV-vis absorption spectra of PBDB-T:IT-M bulk heterojunction thin films fabricated via spin-coating (SC) and doctor blading (DB) in the glovebox and ambient condition. (c) J–V curves and (d) EQE curves of typical spin-coated and doctor-bladed PBDB-T:IT-M OSCs in the glovebox and ambient condition.

TABLE I. Photovoltaic parameters of BHJ OSCs fabricated by spin-coating in the glovebox, spin-coating, and doctor-blading in the ambient condition, respectively. The average PCEs are obtained from 10 devices.

Deposition	V_{oc} (V)	J_{sc} (mAcm ⁻²)	FF (%)	PCE (%)	PCE (Max)
Spin-coating in the glovebox	0.91 ± 0.01	16.31 ± 0.62	67.4 ± 1.9	10.77 ± 0.52	11.92 %
Spin-coating in the ambient condition	0.91 ± 0.01	15.77 ± 0.56	66.2 ± 2.4	9.59 ± 0.19	9.91 %
Doctor-blading in the ambient condition	0.91 ± 0.01	14.39 ± 0.65	65.7 ± 2.7	8.82 ± 0.16	9.00 %

and the statistical parameters are shown in Table I. The spin-coated OSCs fabricated in the glovebox exhibit the highest PCE up to 11.92%, with an open-circuit voltage (V_{oc}) of 0.94 V, a short-circuit current (J_{sc}) of 16.25 mA cm⁻², and a fill factor (FF) of 70.56%. The average PCE is 10.77% with an average V_{oc} of 0.91 V, a J_{sc} of 16.31 mA cm⁻², and a FF of 67.4%. As the fabrication is transferred from the glovebox to the ambient condition, the typical PCE decreases from 11.92% to 9.91% with a V_{oc} of 0.91 V, a J_{sc} of 14.69 mA cm⁻², and a FF of 67.1%. The average V_{oc} is the same, but the FF decreases from 67.4% to 66.2% and J_{sc} decreases from 16.31 mA cm⁻² to 15.77 mA cm⁻², resulting in a decreased average PCE to 9.59%. The average PCE shows an about 11% decrease after transferring the fabrication environment from the glovebox to the ambient condition via spin-coating deposition.

Furthermore, PBDB-T:IT-M OSCs are fabricated via doctor-blading in the ambient condition, which is a R2R compatible large-area deposition technique for potentially practical manufacturing. Impressively, the doctor-bladed OSCs possess good performance as well compared to the spin-coated ones, exhibiting a typical PCE of 9.00% with a V_{oc} of 0.91 V, a J_{sc} of 14.69 mA cm⁻², and a FF of 67.06%. The average V_{oc} does not change. The FF decreases to 65.7%, and the J_{sc} decreases to 14.39 mA cm⁻², resulting in an average PCE of 8.82%, which is just about 7% decrease as compared to spin-coated OSCs in the ambient condition. The results suggest that spin-coated and doctor-bladed OSCs in the ambient condition exhibit similar performance parameters. It should be noticed that the performance parameters of doctor-bladed OSCs in the ambient condition are optimized by varying the substrate temperature. The optimized substrate temperature is set to be 60 °C, resulting in a typical PCE of 9.00%. The typical J - V curves of OSCs fabricated via doctor blading at the different substrate temperatures are shown in Fig. S2, and the corresponding photovoltaic performance parameters are summarized in Table S1. Atomic force microscopy (AFM) images indicate that the blend film fabricated at 60 °C displays a smooth surface with a root mean square (RMS) of 4.05 nm as compared to that of 10.34 nm and 6.72 nm at 50 °C and 70 °C, respectively, resulting in a higher J_{sc} and FF (Fig. S3). The performance parameters of OSC devices with the optimized thickness of the active layer fabricated by doctor blading are shown in Fig. S4 and Table S2. J_{sc} can be improved upon increasing the thickness, resulting from the increased absorption. The optimized thickness of 120 nm produces the device with the best performance. The very thick film would contribute to the increased defect densities and result in FF degradation.

The external quantum efficiency (EQE) curves of OSCs are displayed in Fig. 2(d). All OSC devices show a strong photoresponse from 300 nm to 800 nm, which are consistent with the absorption spectra of PBDB-T:IT-M bulk heterojunction thin films in Fig. 2(b). All the PBDB-T:IT-M thin films have strong absorption bands covering from 550 nm to 750 nm, and the OSC devices have a very high

EQE response in this region with the maximum values. The EQE of the spin-coated PBDB-T:IT-M thin film fabricated in the ambient condition is slightly lower than that of the spin-coated PBDB-T:IT-M thin film fabricated in the glovebox. However, the EQE of the doctor-bladed PBDB-T:IT-M thin film shows higher values from 300 nm to 500 nm as compared with the spin-coated one in the ambient condition, which is consistent with the absorption spectra. The integral current density values (J_{EQE}) deduced from the EQE spectra agree well with those tested from the J - V measurements. The integrated current densities are 15.95 mA cm⁻², 14.48 mA cm⁻², and 13.98 mA cm⁻² for OSCs fabricated via spin-coating in the glovebox, spin-coating in the ambient condition, and doctor-blading in the ambient condition, respectively, which are consistent with the J - V measurements.

The performance of OSCs is closely related to the morphological characteristics and microstructure of the active layer. AFM was carried out to survey the morphology of the blend thin films. As shown in Fig. 3, all the blend thin films exhibit uniform and smooth surface morphologies. The spin-coated PBDB-T:IT-M thin film fabricated in the glovebox displays a quite smooth surface with a relatively small RMS roughness of 2.36 nm, which contributes to the good contact between the MoO₃ and the active layer. However, spin-coated and doctor-bladed PBDB-T:IT-M thin films deposited in the ambient condition show higher RMS values of 3.93 nm and 4.05 nm, respectively. These differences of morphologies in the blend thin films are considered to influence the charge separation and extraction, resulting in different J_{sc} and FF in these three fabrication processes. Furthermore, Then, J_{sc} and V_{oc} under various light intensities were measured to prove the charge recombination in the blend films, and the results are shown in Figs. 3(d) and 3(e). The dependence of J_{sc} on light intensity (P_{light}) can be presented as $J_{sc} \propto P_{light}^{\alpha}$, where $\alpha = 1$ represents the good charge transport with less bimolecular recombination. The α values of devices with the blend thin films fabricated by spin-coating in the glovebox, spin-coating, and doctor-blading in the ambient condition are calculated to be 0.952, 0.925, and 0.917, suggesting that the bimolecular recombination occurred more seriously in blend thin films prepared by spin-coating and doctor-blading in the ambient condition. Moreover, the relationship between V_{oc} and P_{light} can be described as $V_{oc} \propto nkT/e \ln(P_{light})$ (k represents Boltzmann's constant, T is the absolute temperature, and e is the elementary charge) and the slope reflects the trap-assisted recombination. The slopes are calculated to be 1.704 kT/e, 1.781 kT/e, and 1.792 kT/e for the blend thin films fabricated by spin-coating in the glovebox, spin-coating, and doctor-blading in the ambient condition, respectively, implying that the trap-assisted recombination of spin-coated devices in the glovebox is less than spin-coated and doctor-bladed devices in the ambient condition. Consequently, the higher J_{sc} and FF of spin-coated devices in the glovebox might contribute to the weak bimolecular recombination and trap-assisted recombination.

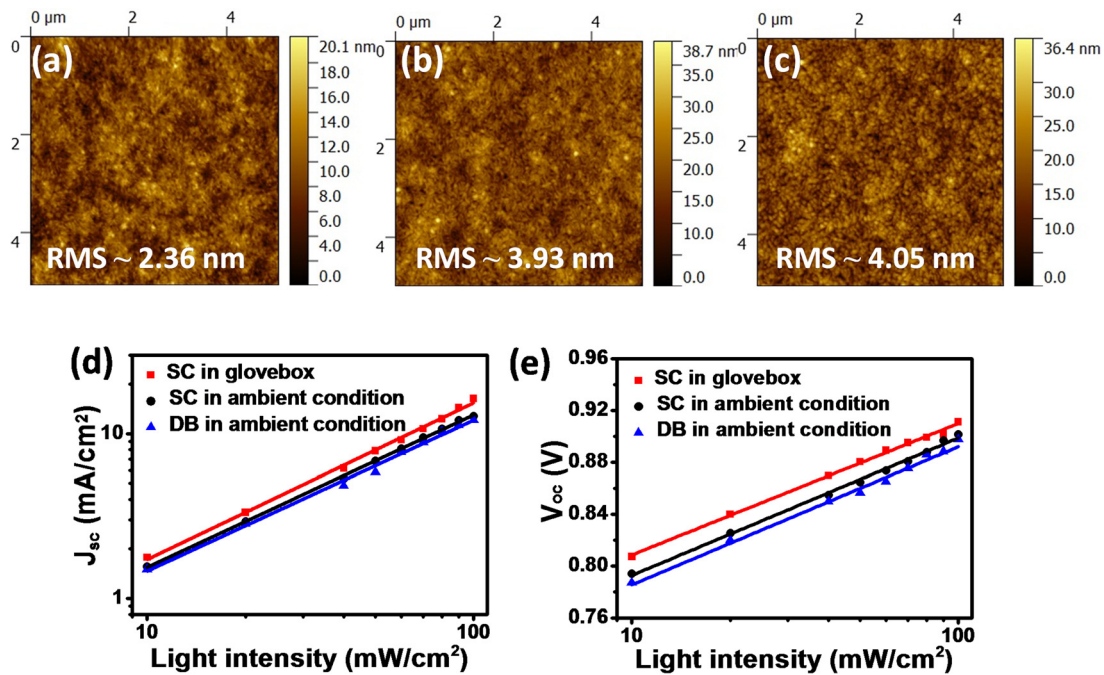


FIG. 3. AFM images of PBDB-T:IT-M thin films fabricated via (a) spin-coating in the glovebox, (b) spin-coating in the ambient condition, and (c) doctor-blading in the ambient condition, respectively. Dependence of J_{sc} (d) and V_{oc} (e) on light intensity of devices with PBDB-T:IT-M thin films fabricated via spin-coating in the glovebox, spin-coating in the ambient condition, and doctor-blading in the ambient condition.

The microstructure of PBDB-T:IT-M thin films was measured by GIWAXS. The two-dimensional (2D) GIWAXS patterns of PBDB-T:IT-M thin films fabricated by spin-coating and doctor-blading in the glovebox and ambient condition are illustrated in Figs. 4(a)–4(c). Figures 4(d) and 4(e) show the corresponding results of out-of-plane and in-plane GIWAXS profiles, respectively. In Fig. 4(d), all thin films show a pronounced peak located at the same position around $q = 2.98 \text{ nm}^{-1}$, which is attributed to the (100) lamellar stacking peak of the PBDB-T, corresponding to the good self-assembly of PBDB-T.³⁸ The intensity of the peak decreases dramatically in blend thin films fabricated by spin-coating and doctor-blading in the ambient condition as compared to the blend thin film prepared via spin-coating in the glovebox. The identical peak position for the (100) lamellar packing could also be observed in the in-plane direction [Fig. 4(e)], and the intensity change trend is the same as the in-plane diffraction peak. Meanwhile, a diffraction peak at about 3.90 nm^{-1} for IT-M appears when the blend thin films were fabricated via spin-coating in the glovebox and ambient condition, while this peak is absent in the doctor-bladed thin film [Fig. 4(d)]. It is demonstrated that the crystallization of both spin-coated PBDB-T:IT-M thin films is enhanced, exhibiting a stronger crystallization than that of the doctor-bladed thin film. The relatively low crystallinity for the blend thin film via doctor-blading in the ambient condition could decrease charge transport, which is consistent with the lower J_{sc} and FF . Although spin-coated thin films can promote crystallization, the doctor-bladed thin film still shows good properties. It means that doctor-blading can produce a smooth and uniform thin film; especially, it can be compatible with representative large-area, roll-to-roll deposition of OSCs.

The space charge limited current (SCLC) measurement was employed to detect the charge transport properties of the blend thin films, as shown in Fig. S5 and Table S3. For the blend thin films fabricated by spin-coating in the glovebox, hole mobility (μ_h) and electron mobility (μ_e) are measured to be $2.68 \times 10^{-4} \text{ cm}^2 \text{ V}^{-1} \text{ s}^{-1}$ and $9.99 \times 10^{-4} \text{ cm}^2 \text{ V}^{-1} \text{ s}^{-1}$, respectively. μ_h and μ_e are measured to be $1.99 \times 10^{-4} \text{ cm}^2 \text{ V}^{-1} \text{ s}^{-1}$ and $6.35 \times 10^{-4} \text{ cm}^2 \text{ V}^{-1} \text{ s}^{-1}$, respectively, for the blend thin film fabricated via spin-coating in the ambient condition. Furthermore, μ_h and μ_e are measured to be $1.95 \times 10^{-4} \text{ cm}^2 \text{ V}^{-1} \text{ s}^{-1}$ and $4.34 \times 10^{-4} \text{ cm}^2 \text{ V}^{-1} \text{ s}^{-1}$, respectively, for the blend thin films prepared via doctor-blading in the ambient condition. The blend thin film fabricated by spin-coating in the glovebox exhibits higher μ_h and μ_e than the ones prepared by spin-coating and doctor-blading in the ambient condition, indicating that charge transport in the blend thin film fabricated by spin-coating in the glovebox would contribute to the higher J_{sc} and FF .

Film-depth-dependent light absorption can be used to analyze the vertical phase segregation of active layers in BHJ OSCs.³⁹ It is well known that each sublayer has different morphology and light absorption, which is effectively manipulated by the different fabrication conditions. Thus, the film-depth-dependent light absorption is used to study the light absorption and vertical phase segregation of PBDB-T:IT-M active layers. The schematic is shown in Fig. S6. Plasma etching is utilized to acquire the film-depth-dependent light absorption spectra with a nanometer depth resolution. It was reported that etching by oxygen plasma could remove part of the film, thus reducing the light absorption of the film.⁴⁰ The etching of polymers by low-pressure oxygen plasma is highly surface-selective and not easy to

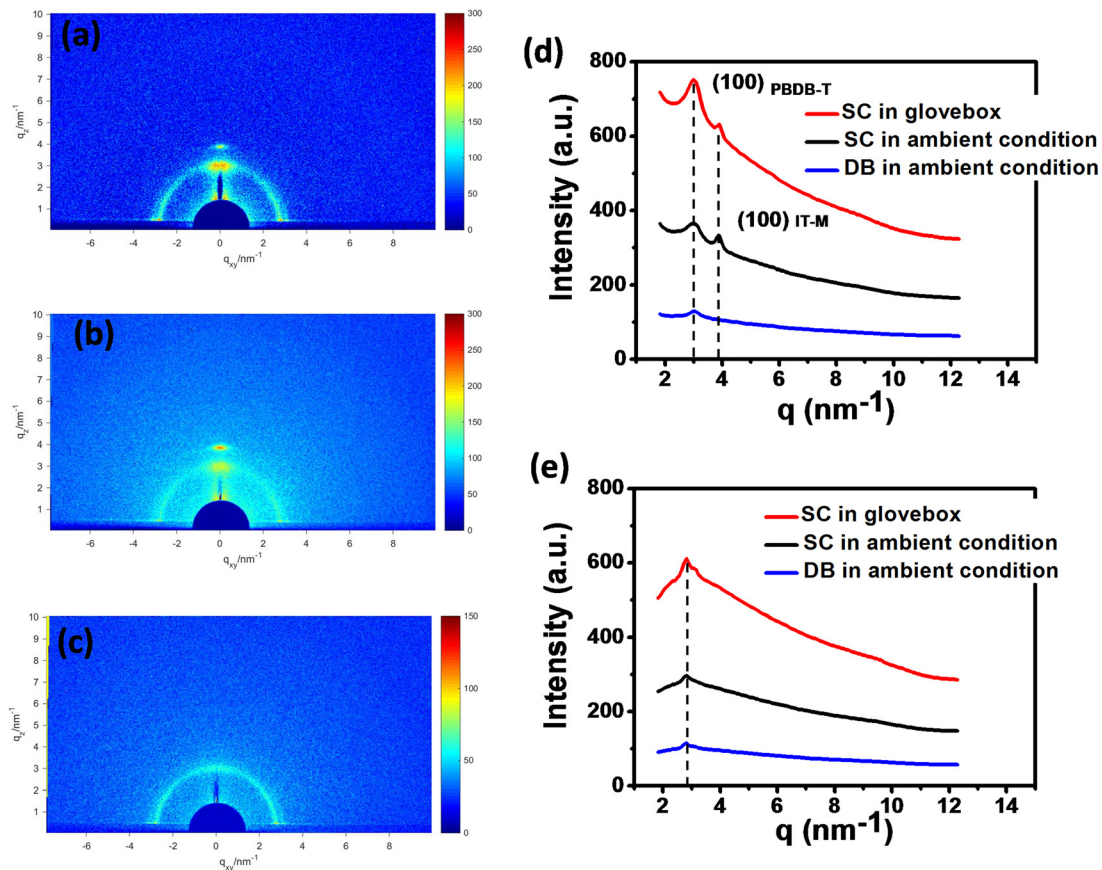


FIG. 4. 2D GIWAXS patterns of PBDB-T:IT-M thin films fabricated via (a) spin-coating in the glovebox, (b) spin-coating in the ambient condition, and (c) doctor-blading in the ambient condition. (d) and (e) The corresponding results of out-of-plane and in-plane GIWAXS profiles, respectively.

oxidize the sub-surface material during etching.⁴¹ Figures 5(a)–5(c) show the light absorption spectra of PBDB-T:IT-M blend thin films at different depths of thin films, and each spectrum is from the different sublayers. The PBDB-T:IT-M thin films present the vertical phase variation owing to the different phase evolution between air/active-layer and active-layer/ZnO interfaces during the different deposition processes. The film-depth-dependent composition, as extracted from the film-depth-dependent absorption spectra, is displayed along the film depth directions of active layers [Figs. 5(d)–5(f)], where the depths 0 and 100 nm represent the active-layer/MoO₃ and active-layer/ZnO interfaces, respectively. In three cases, the contents of donor PBDB-T in the half part of the blend thin film at a depth 0~25 nm (near MoO₃) are about 60–70 wt. %, while the contents of acceptor IT-M are about 30–40%. The donor is dominated in the region near MoO₃, providing sufficient conductive pathways for the hole transport toward the MoO₃/Ag electrode. For all of the three films, the donor content at the top half part (near MoO₃) of the film is higher than that at the bottom half part (near ZnO), which is beneficial to the high photovoltaic performance with an inverted device configuration [Figs. 5(g)–5(i)]. Close to the ZnO side, the content of acceptor IT-M at a depth 75–100 nm is about ~50 wt. % for the PBDB-T:IT-M thin film deposited via spin-coating in the glovebox [Fig. 5(d)]. While the contents

decrease to about 45 wt. % and 40 wt. % for PBDB-T:IT-M thin films deposited via spin-coating [Fig. 5(e)] and doctor-blading in the ambient condition [Fig. 5(f)], respectively. It means that the acceptor is not dominated in the region near ZnO, and the single-phase aggregation of the donor is large, resulting in suppressing exciton separation, which is not helpful to the electron extraction and transport toward the ZnO/Ag electrode. It should be the important reason that the J_{sc} obviously decreases for PBDB-T:IT-M OSCs fabricated in the ambient condition. As discussed above, the PBDB-T:IT-M blend thin films fabricated in the glovebox via spin-coating have a clear feature with a better interpenetrating network, which could decrease surface bimolecular recombination and improve the charge mobility. However, PBDB-T:IT-M thin films deposited in the ambient condition do not show the distribution over 50% close to the active-layer/ZnO interface, which definitely influences the device performance. It obviously indicates that the fabrication environment greatly influences the microphase separation of PBDB-T:IT-M thin films and, accordingly, the device performance. Furthermore, the absorption of the blend thin film fabricated via spin coating in the glovebox shows a relatively broad peak between 300 nm to 500 nm [Fig. 5(g)]. However, in the same range, the absorption spectra of the blend thin film via spin-coating and doctor-blading in the ambient condition are displayed

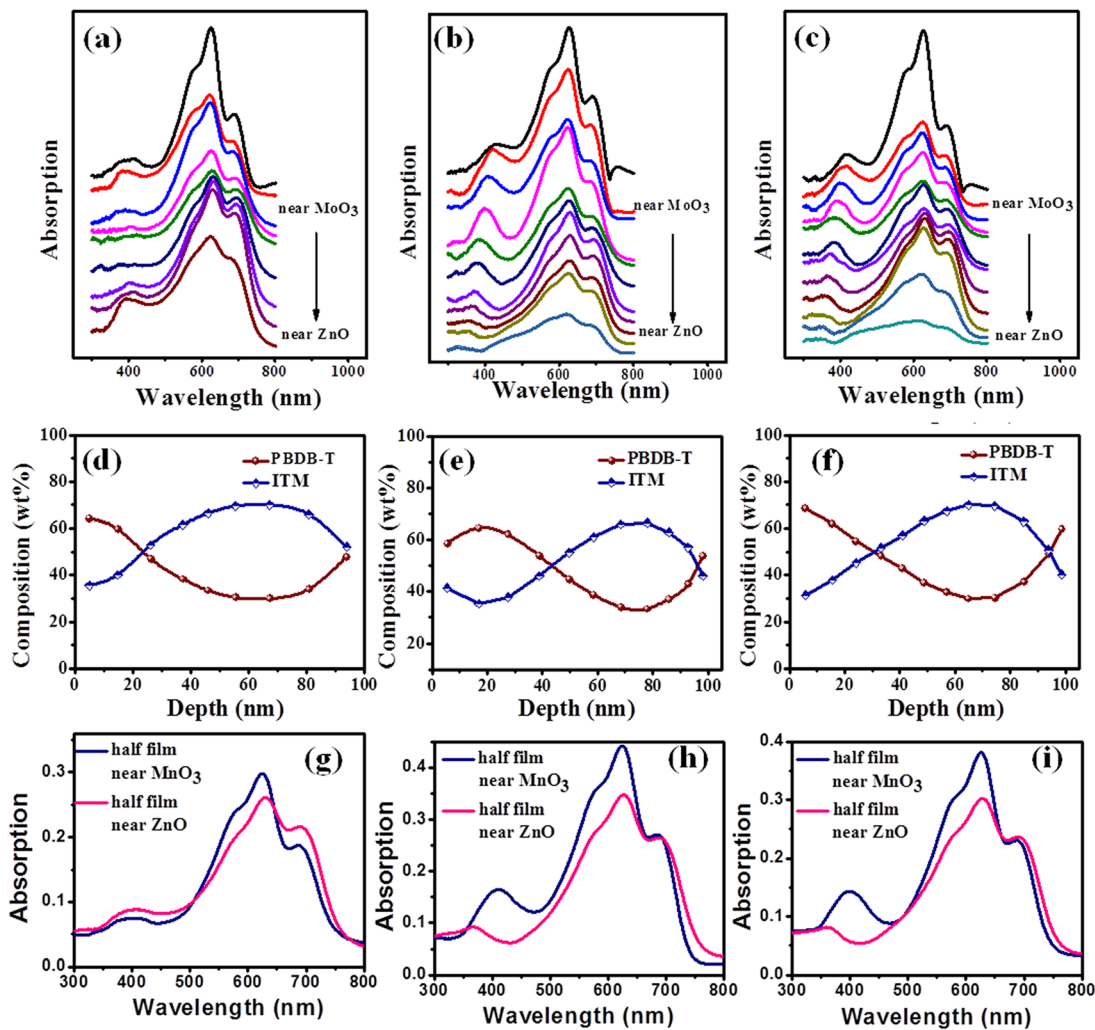


FIG. 5. Film-depth-dependent variation of PBDB-T:IT-M thin films. (a)–(c) Film-depth-dependent light absorption spectra of PBDB-T:IT-M thin films fabricated via spin-coating in the glovebox (a), spin-coating in the ambient condition (b), and doctor-blading in the ambient condition (c), respectively. As a guide to the eye, the spectra are shifted along the vertical direction. Each spectrum denotes the absorption of a sublayer with a comparable thickness. (d)–(f) Composition distribution profile as a function of film depth for PBDB-T:IT-M thin films fabricated via spin-coating in the glovebox (d), spin-coating in the ambient condition (e), and doctor-blading in the ambient condition (f), respectively. The profiles were obtained from film-depth-dependent spectra. (g)–(i) Light absorption spectra of half-films fabricated via spin-coating in the glovebox (g), spin-coating in the ambient condition (h), and doctor-blading in the ambient condition (i), respectively. The thin film is tentatively assumed to be divided into two half-films, namely, a half-film near MoO₃ and a half-film near ZnO.

with obvious shoulders [Figs. 5(h) and 5(i)], implying that the donor PBDB-T distributes more on the top part of blend thin films, which is consistent with the previous absorption analysis.

In order to further understand the photovoltaic performances of the OSC, electrochemical impedance spectroscopy (EIS) analysis was conducted to study the electrical dynamics, and the equivalent circuit model is presented in Fig. S7(a). As shown in Fig. S7(b), the impedance spectroscopy of OSCs fabricated by spin-coating in the glovebox shows the smallest charge-transfer resistance (R_{ct}) as compared to the ones fabricated by spin-coating and doctor-blading in the ambient condition. Meanwhile, it is worth pointing out that the series resistance (R_s) of the spin-coated device in the glovebox is smaller than that of spin-coated and doctor-bladed ones in the ambient condition.

It suggests that the spin-coated device in the glovebox has good contact between the ZnO layer and the active layer. These results also explain the photovoltaic performance parameters of OSCs fabricated via three different conditions, especially for the J_{sc} and FF .

In summary, PBDB-T:IT-M OSC devices fabricated via spin-coating and doctor-blading in the glovebox and ambient condition were studied in detail. The fabrication environment greatly affects the morphology, microphase separation, crystallinity, and microstructure of the deposited PBDB-T:IT-M thin films and, accordingly, influences the performance parameters of OSCs. A PCE of up to 9.00% could be obtained for OSCs fabricated via doctor-blading in the ambient condition, which is nearly comparable to spin-coated OSCs in the ambient condition with a PCE of 9.91%. The fabrication transferring from the

glovebox via spin-coating to the ambient condition via doctor-blading demonstrated that efficient OSCs could be fabricated via large-scale, low-cost doctor-blading in the ambient condition, which is compatible with industrial production of the R2R process.

See the [supplementary material](#) for the experimental details; UV-vis absorption spectra of PBDB-T and IT-M thin films; J - V curves of PBDB-T:IT-M OSCs prepared by doctor-blading at the different substrate temperatures; photovoltaic parameters of PBDB-T:IT-M OSCs prepared by doctor-blading at the different substrate temperatures measured under the illumination of AM1.5G, 100 mW cm⁻²; AFM images of PBDB-T:IT-M thin films fabricated via doctor-blading in the ambient condition at 50 °C, 60 °C, and 70 °C; $J^{1/2}$ - V plots for the hole-only devices and for the electron-only devices; hole and electron mobilities for the blend thin films fabricated by three different conditions; schematic of film-depth-dependent light absorption; equivalent-circuit model employed for the EIS fitting of OSCs; and Nyquist plots (symbols) and fitting curves (solid lines) of OSCs.

This work was supported by the National Key Research and Development Program of China (No. 2017YFA0206600) and the National Natural Science Foundation of China (No. 51673214). H.Y.L. also acknowledges the support from the Key Innovation Project of Graduate of Central South University (Grant No. 2018ZZTS106).

DATA AVAILABILITY

The data that support the findings of this study are available from the corresponding author upon reasonable request.

REFERENCES

- Z. Xiao, S. F. Yang, Z. Yang, J. L. Yang, H. L. Yip, F. J. Zhang, F. He, T. Wang, J. Z. Wang, Y. B. Yuan, H. Yang, M. K. Wang, and L. M. Ding, *Adv. Mater.* **31**, 1804790 (2019).
- J. L. Yang, D. Vak, N. Clark, J. Subbiah, W. W. H. Wong, D. J. Jones, S. E. Watkins, and G. Wilson, *Sol. Energy Mater. Sol. Cells*, **109**, 47 (2013).
- J. Xiong, B. C. Yang, C. H. Zhou, J. L. Yang, H. C. Duan, W. L. Huang, X. Zhang, X. D. Xia, L. Zhang, H. Huang, and Y. L. Gao, *Org. Electron.* **15**, 835 (2014).
- C. J. Zhang, Q. Luo, H. Wu, H. Y. Li, J. Q. Lai, G. Q. Ji, L. P. Yan, X. F. Wang, D. Zhang, J. Lin, L. W. Chen, J. L. Yang, and C. Q. Ma, *Org. Electron.* **45**, 190 (2017).
- X. P. Xu, K. Feng, Z. Z. Bi, W. Ma, G. G. Zhang, and Q. Peng, *Adv. Mater.* **31**, 1901872 (2019).
- J. F. Wei, C. J. Zhang, G. Q. Ji, Y. F. Han, I. Ismail, H. Y. Li, Q. Luo, J. L. Yang, and C. Q. Ma, *Sol. Energy* **193**, 102 (2019).
- J. Xiong, B. C. Yang, C. H. Cao, R. S. Wu, H. C. Duan, Y. L. Huang, J. Sun, J. Zhang, C. B. Liu, S. H. Tao, Y. L. Gao, and J. L. Yang, *Org. Electron.* **30**, 30 (2016).
- F. Zhao, S. Dai, Y. Wu, Q. Zhang, J. Wang, L. Jiang, Q. Ling, Z. Wei, W. Ma, W. You, C. Wang, and X. Zhan, *Adv. Mater.* **29**, 1700144 (2017).
- J. Xiong, J. L. Yang, B. C. Yang, C. H. Zhou, H. P. Xie, H. Huang, and Y. L. Gao, *Org. Electron.* **15**, 1745 (2014).
- H. Y. Li, C. J. Zhang, J. F. Wei, K. Q. Huang, X. T. Guo, Y. Yang, S. K. So, Q. Luo, C. Q. Ma, and J. L. Yang, *Flexible Printed Electron.* **4**, 044007 (2019).
- H. W. Hu, P. C. Y. Chow, G. Y. Zhang, T. X. Ma, J. Liu, G. F. Yang, and H. Yan, *Acc. Chem. Res.* **50**, 2519 (2017).
- Z. Z. Zhang, L. L. Feng, S. T. Xu, Y. Liu, H. J. Peng, Z. G. Zhang, Y. F. Li, and Y. P. Zou, *Adv. Sci.* **4**, 1700152 (2017).
- W. Zhao, S. Li, H. Yao, S. Zhang, Y. Zhang, B. Yang, and J. Hou, *J. Am. Chem. Soc.* **139**, 7148 (2017).
- F. Wei, G. Q. Ji, C. J. Zhang, L. P. Yan, Q. Luo, C. Wang, Q. Chen, J. L. Yang, L. W. Chen, and C. Q. Ma, *ACS Nano* **12**, 5518 (2018).
- Q. Q. Zhang, M. A. Kelly, N. Bauer, and W. You, *Acc. Chem. Res.* **50**, 2401 (2017).
- M. Q. Pan, T. K. Lau, Y. B. Tang, Y. C. Wu, T. Liu, K. Li, M. C. Chen, X. H. Lu, W. Ma, and C. L. Zhan, *J. Mater. Chem. A* **7**, 20713 (2019).
- L. X. Meng, Y. M. Zhang, X. J. Wan, C. X. Li, X. Zhang, Y. B. Wang, X. Ke, Z. Xiao, L. M. Ding, R. X. Xia, H. L. Yip, Y. Cao, and Y. S. Chen, *Science* **361**, 1094 (2018).
- B. S. S. Pokuri, J. Sit, O. Wodo, D. Baran, T. Ameri, C. J. Brabec, A. J. Moule, and B. Ganapathysubramanian, *Adv. Energy Mater.* **7**, 1701269 (2017).
- H. Kang, G. Kim, J. Kim, S. Kwon, H. Kim, and K. Lee, *Adv. Mater.* **28**, 7821 (2016).
- Y. Diao, L. Shaw, Z. N. Bao, and S. C. B. Mannsfeld, *Energy Environ. Sci.* **7**, 2145 (2014).
- H. Zhong, L. Ye, J.-Y. Chen, S. B. Jo, C.-C. Chueh, J. H. Carpenter, H. Ade, and A. K. Y. Jen, *J. Mater. Chem. A* **5**, 10517 (2017).
- X. Liu, L. Nian, K. Gao, L. Zhang, L. Qing, Z. Wang, L. Ying, Z. Xie, Y. Ma, Y. Cao, F. Liu, and J. Chen, *J. Mater. Chem. A* **5**, 17619 (2017).
- S. B. Dkhil, M. Pfannmoller, S. Bals, T. Koganezawa, N. Yoshimoto, D. Hannani, M. Gaceur, C. V. Ackermann, O. Margeat, and J. Achkermann, *Adv. Energy Mater.* **6**, 1600290 (2016).
- X. F. Liao, L. Zhang, X. T. Hu, L. Chen, W. Ma, and Y. W. Chen, *Nano Energy* **41**, 27 (2017).
- C. Kapnopoulos, E. D. Mekeridis, L. Tzounis, C. Polyzoidis, A. Zachariadis, S. Tsimikli, C. Gravalidis, A. Laskarakis, N. Vouroutzis, and S. Logothetidis, *Sol. Energy Mater. Sol. Cells* **144**, 724 (2016).
- H. W. Ro, J. M. Downing, S. Engmann, A. A. Herzing, D. M. DeLongchamp, L. J. Richter, S. Mukherjee, H. Ade, M. Abdelsamie, L. K. Jagadamma, A. Amassian, Y. H. Liu, and H. Yan, *Energy Environ. Sci.* **9**, 2835 (2016).
- S. Mukherjee, A. A. Herzing, D. L. Zhao, Q. H. Wu, L. P. Yu, H. Ade, D. M. DeLongchamp, and L. J. Richter, *J. Mater. Res.* **32**, 1921 (2017).
- D. Vak, K. Hwang, A. Faulks, Y. S. Jung, N. Clark, D. Y. Kim, G. J. Wilson, and S. E. Watkins, *Adv. Energy Mater.* **5**, 1401539 (2015).
- Q. Hu, H. Wu, J. Sun, D. Yan, Y. Gao, and J. Yang, *Nanoscale* **8**, 5350 (2016).
- H. Wu, C. Zhang, K. Ding, L. Wang, Y. Gao, and J. Yang, *Org. Electron.* **45**, 302 (2017).
- L. Ye, Y. Xiong, H. F. Yao, A. Gadisa, H. Zhang, S. S. Li, M. Ghasemi, N. Balar, A. Hunt, B. T. O'Connor, J. H. Hou, and H. Ade, *Chem. Mater.* **28**, 7451 (2016).
- K. Zhao, H. Hu, E. Spada, L. K. Jagadamma, B. Yan, M. Abdelsamie, Y. Yang, L. Yu, R. Munir, R. Li, G. O. N. Ndjawa, and A. Amassian, *J. Mater. Chem. A* **4**, 16036 (2016).
- X. Zhan, A. Facchetti, S. Barlow, T. J. Marks, M. A. Ratner, M. R. Wasielewski, and S. R. Marder, *Adv. Mater.* **23**, 268 (2011).
- Y. B. Lin, Y. Z. Jin, S. Dong, W. H. Zheng, J. Y. Yang, A. Liu, F. Liu, Y. F. Jiang, T. P. Russell, F. L. Zhang, F. Huang, and L. T. Hou, *Adv. Energy Mater.* **8**, 1701942 (2018).
- L. Zhang, B. J. Lin, B. Hu, X. B. Xu, and W. Ma, *Adv. Mater.* **30**, 1800343 (2018).
- S. I. Na, Y. H. Seo, Y. C. Nah, S. S. Kim, H. Heo, J. E. Kim, N. Rolston, R. H. Dauskardt, M. Gao, Y. Lee, and D. Vak, *Adv. Funct. Mater.* **29**, 1805825 (2019).
- E. Destouesse, M. Top, J. Lamminaho, H. G. Rubahn, J. Fahlteich, and M. Madsen, *Flexible Printed Electron.* **4**, 045004 (2019).
- W. Li, J. L. Cai, Y. Yan, F. L. Cai, S. S. Li, R. S. Gurney, D. Liu, J. D. McGettrick, T. M. Watson, Z. Li, A. J. Pearson, D. G. Lidzey, J. H. Hou, and T. Wang, *Sol. RRL* **2**, 1800114 (2018).
- J. Y. Wang, J. X. Zhang, Y. Q. Xiao, T. Xiao, R. Y. Zhu, C. Q. Yan, Y. Q. Fu, G. H. Lu, X. H. Lu, S. R. Marder, and X. W. Zhan, *J. Am. Chem. Soc.* **140**, 9140 (2018).
- G. H. Lu, J. C. Blakesley, S. Himmelberger, P. Pingel, J. Frisch, I. Lieberwirth, I. Salzmann, M. Oehzelt, R. D. Pietro, A. Salleo, N. Koch, and D. Neher, *Nat. Commun.* **4**, 1588 (2013).
- L. J. Bu, S. Gao, W. C. Wang, L. Zhou, S. Feng, X. Chen, D. M. Yu, S. T. Li, and G. H. Lu, *Adv. Electron. Mater.* **2**, 1600359 (2016).